ARTICLE

Computational Fluid Dynamic (CFD) and Reaction Modelling Study of Bio-oil Catalytic Hydrodeoxygenation in Microreactors

Sanaa Hafeez,[a] Elsa Aristodemou,[a,b] George Manos,[c] S.M. Al Salem,[d] and Achilleas Constantinou[*a,c,e]

Received 00th January 20xx,
Accepted 00th January 20xx

DOI: 10.1039/x0xx00000x

A Computational Fluid Dynamic (CFD) model was derived and validated, in order to, investigate the hydrodeoxygenation reaction of 4-propylguaiacol, which is a lignin-derived compound present in bio-oil. A 2-D packed bed microreactor was simulated using pre-sulphided $NiMo/Al_2O_3$ solid catalyst in isothermal operation. A pseudo-homogeneous model was first created to validate the experimental results from literature. Various operational parameters were investigated and validated with the experimental data, such as temperature, pressure and liquid flow rate; and it was found that the CFD findings were in very good agreement with the results from literature. The model was then upgraded to that of a detailed multiphase configuration; and phenomena such as internal and external mass transfer limitations were investigated, as well as, reactant concentrations on the rate of 4-propylguaiacol. Both models agreed with the experimental data, and therefore confirm their ability for applications related to the prediction of the behaviour of bio-oil compounds hydrodeoxygenation.

1. Introduction

Biomass presents numerous advantages as a renewable feedstock for bio-fuels. It contains low sulphur and nitrogen and presents its self as a lucrative alternative due to its lack of net carbon dioxide (CO_2) emissions to the environment[1]. Resources from biomass consist of a vast range of materials such as organic waste products, forest and agricultural residues and energy crops[2]. Biomass feedstock's which contain cellulose, hemicellulose and lignin possess a high-energy content, and are often converted to oil using fast pyrolysis[2, 3].

Fast pyrolysis is the process of rapidly heating biomass under moderately high temperature conditions of around 500 ^oC and short reaction times of 2 seconds, in the absence of oxygen. In return, biomass degrades to produce mainly vapours, aerosols and some solid char. After processing, a dark brown liquid is obtained which has a heating value of approximately half of that of conventional fuel oil averaging at about 30 MJ kg^{-1} [4]. Biomass derived bio-oil has several disadvantages such as a low heating value, high viscosity and a high oxygen content, which all restrict its application as a liquid fuel. Therefore, further upgrading of bio-oil by hydrodeoxygenation (HDO) is required[5].

The HDO process converts the oxygen containing compounds such as acids, aldehydes, alcohols and phenol to oxygen-free hydrocarbon fuels[6]. Bio-oil obtained from the fast pyrolysis of lignin contains approximately 39% of guaiacol and its derivatives. Amongst these constituents, guaiacol is often regarded as a representative model for bio-oil derived from lignin because it has two types of C-O bonds (Csp_2OH and Csp_2OCH_3) within its molecular structure[7]. Based on this, majority of studies have utilised the compound guaiacol as a model compound and have investigated the HDO of guaiacol using catalysts such as $NiMo/Al_2O_3$ and $CoMo/Al_2O_3$, precious metal catalysts, such as platinum, ruthenium and rhodium, and nickel (Ni) catalyst[8].

Phenolic compounds such as guaiacol, anisol and phenol have been extensively modelled in past studies due to their significant present in bio-oil[6]. Despite this, not much attention has been dedicated to lignin-derived compounds. Therefore, there exists a limited understanding of the reaction pathways and kinetics of the HDO reaction. The study of 4-propylguaiacol HDO has been selected as a basis to produce a model representing lignin-derived compounds[3]. 4-Propylguaiacol represents some of the key lignin-derived components present in bio-oil such as benzene, phenol, guaiacol, anisole, propyl anisole, propylphenol, and propylbenzene. The existence of phenolic compounds in the bio-oil is the origin of polymerisation and coke formation during HDO at elevated temperatures greater than 300^oC[3].

Lee et al.[8] studied the HDO of a model compound of lignin-derived bio-oil (guaiacol) because of its high potential to be used as a substitute for conventional fuels. Platinum-loaded HY zeolites (Pt/HY) with varying Si/AL molar ratios were used as catalysts for the HDO of guaiacol, anisole, veratrole and phenol

[a] Division of Chemical & Petroleum Engineering, School of Engineering, London South Bank University, London SE1 0AA, UK. Email: constaa8@lsbu.ac.uk; Tel: +44(0)20 7815 7185
[b] Department of Earth Sciences, Imperial College London, London, SW7 2AZ, UK.
[c] Department of Chemical Engineering, University College London, London WCIE 7JE, UK.
[d] Environment & Life Sciences Research Centre, Kuwait Institute for Scientific Research, P.O. Box: 24885, Safat 13109, Kuwait.
[e] Department of Chemical Engineering Cyprus University of Technology, 57 Corner of Athinon and Anexartisias, 3036 Limassol, Cyprus

to a variety of hydrocarbons, such as cyclohexane. They found that cyclohexane was the predominant product and the yield increased with increasing number of acid sites. In order to obtain bio-oil with the maximum yield of cyclohexane and alkylated cyclohexanes, the SI/AL molar ratio should be adjusted to balance the Pt particle-induced hydrogenation with acid site-induced methyl group transfer.

Patil et al.[9] studied the HDO of the model compound guaiacol in bio-oil to produce fuel grade oil, using a bimetal catalyst Ni-Mo/ZrO_2-Al_2O_3. The results showed that the conversion of guaiacol and the product yield of phenol and cyclohexane was found to increase with increasing Mo content (10%, 15%, and 20%) at continuous Ni (4%) loading and Ni content (2%, 4%, and 6%) at continuous Mo (20%) loading. However, there was a lower difference in guaiacol conversion and phenol and cyclohexane yield at variable Ni loading. Guaiacol conversion was 100% at 330°C and 30 bars for the improved catalyst.

Taghvaei and Rahimpour[10] investigated the catalytic HDO of guaiacol via a combination of dielectric barrier discharge (DBD) and catalyst. It was found that the highest conversion of guaiacol (92%) and deoxygenation degree of 65% are achieved in the presence of Pt-Cl/Al_2O_3 and Pt-Re/Al_2O_3 catalysts respectively. The predominant products obtained were BTX, phenol, methylphenols and dimethylphenols. It was concluded that the difficulties of using hydrogen for the HDO reaction can be overcome by using the catalytic DBD reactor.

Liu et al.[5] investigated the HDO of bio-oil model compounds over amorphous NiB/SiO_2-Al_2O_3 catalyst. The performance of the catalysts was evaluated in an oil-water biphasic system using anisole and guaiacol as the selected model compounds of bio-oil. The results showed that increasing the reaction temperature or reaction time would enhance the conversion of guaiacol and anisole. The HDO pathways of guaiacol and anisole were studied which provided a reference for the HDO mechanism of bio-oil.

Microreactors present numerous advantages to investigate the reaction of HDO. Their enhanced surface-area-to-volume-ratio leads to a much-improved mass and heat transfer, in addition to, shorter residence time. Therefore, reactions which contain unstable intermediates are better suited to these type of reactors because of their stability and high degree of control[11]. These collective advantages of microreactors mean that they are greener and environmentally sustainable[12].

In order to understand the effects of HDO on the further processing of bio-oil several studies have identified mathematical modelling exercises to fully simulate its interaction with compounds under various conditions[13-16]. The majority of HDO studies have focused on sulphided cobalt and nickel-based molybdenum (CoMo and NiMo) based catalysts for the separation of sulphur, nitrogen and oxygen from petrochemical feedstocks[17].

The catalytic HDO reaction of 4-propylguaiacol to 4-propylphenol using pre-sulphided NiMo/Al_2O_3 catalyst is investigated and presented in this study using a packed-bed plug flow microreactor. A pseudo homogeneous model was produced, and good model validation was obtained with the experimental data. In this study, a 2-D Computational Fluid Dynamic (CFD) model was created to improve the understanding of the mass transfer and catalytic reactions taking place within the microreactor and provide an insight into any potential improvements that could be made by investigating these parameters. A validation of the model with the experimental data from literature[3] is shown, and further investigations such as, internal and external mass transfer are conducted herein.

2. Modelling Methodology

2.1 Reaction kinetics

The reaction considered for the CFD mathematical modelling is the HDO of 4-propylguaiacol to 4-propylphenol (eq. 1). The kinetic studies from the experiment suggest that the kinetics for the reaction are determined by the surface reaction step which represent the competitive reaction with non-dissociative adsorption of hydrogen[3]. The kinetics were determined using the Langmuir-Hinshelwood-Hougen-Watson (LHHW) method, thus giving the rate equation shown below:

$$C_{10}H_{14}O_2 + H_2 \rightarrow C_9H_{12}O + CH_3OH \quad (1)$$

$$-r'_{4PG} = \frac{k(K_{H_2}{}^{eql}C_{H_2})(K_{4PG}{}^{eql}C_{4PG})}{(1+K_{H_2}{}^{eql}C_{H_2})(1+K_{4PG}{}^{eql}C_{4PG})} \quad (2)$$

where *k* is the kinetic rate constant of each reaction pathway (L mol^{-1}) and C is the molar concertation at each stage of reaction mechanism. Readers are referred to Joshi and Lawal, 2013 for the reaction scheme. From the rate expression, it can be deduced that the reaction is pseudo-first-order with respect to 4-propylguaiacol and hydrogen. Table 1 displays the kinetic constants utilised for the study, and Table 2 conveys the pre-exponential factors, activation energies and heats of adsorption upon which the CFD modelling is based.

2.2 Pseudo-homogeneous model

The microreactor models were simulated using CFD to demonstrate the particle-fluid transport phenomena. Experimental work is typically costly and time-consuming, while multiphase CFD studies can deliver comprehensive information on the spatiotemporal variations in species flows, concentrations and temperatures within the reactor and with minimal effort. Therefore, CFD is a favourable approach/methodology predicting the parameters thus, enabling a detailed study of the physico-chemical processes involved[16]. CFD is an integrated methodology in the package that was used.

Table 1: Reaction kinetics parameters and rate constants used as input parameters for the described model. Source:[3].

T (°C)	k (mol $g^{-1}h^{-1}$)	K_{4PG} (L mol^{-1})	K_{H2} (L mol^{-1})	R^2
250	22.21 ± 0.77	0.02 ± 0.002	0.3 ± 0.004	0.97
300	41.40 ± 4.21	0.1 ± 0.01	0.1 ± 0.01	0.96
350	77.78 ± 0.01	0.6 ± (9.7 × 10^{-5})	0.02 ± (1.6× 10^{-6})	0.96

Table 2: Reaction Pre-exponential factors, activation energy and heats of adsorption Source:[3].

Intrinsic constant	Value
Pre-exponential factors	
k_0 (× 10^4 mol $g^{-1}h^{-1}$)	5.29 ± 0.66
$K_{4-Propylguaiacol,0}$ (× 10^7 L mol^{-1})	2.750 ± 0.14
$K_{H2,0}$ (× 10^{-8} L mol^{-1})	1.6 ± 0.13
Activation energies and heats of adsorption	
E_a (kJ mol^{-1})	33.86 ± 2.70
$\Delta H_{4-Propylguaiacol}$ (kJ mol^{-1})	91.85 ± 2.69
ΔH_{H2} (kJ mol^{-1})	-72.69 ± 2.63

A 2-D microreactor model was created based on the assumption that the concentration and temperature gradients occur only in the axial direction. The only transport mechanism operating in this direction is the overall flow itself, and this is of plug flow type. Further assumptions which the model was founded upon are (a) Application of steady-state and isothermal conditions; (b) there is a pressure drop of 0.07 MPa along the length of the microreactor; (c) Henrys law applies is valid for the gas-liquid interface; (d) the ideal gas law applies for the fluids in the gas phase; and that (d) there is a constant axial fluid velocity in the gas phase with uniform physical properties and transport coefficients. The microreactor has a height of 0.762 mm, and a length of 180 mm. The catalyst used is a pre-sulphided NiMo/Al2O3 in the form of solid spherical particles. Figure 1 shows a schematic diagram of the model used for the simulation.

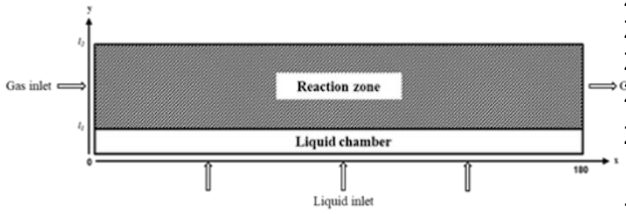

Figure 1: Microreactor model used for the CFD simulation. Note to readers: The schematic is not to scale.

2.3. Mass balances in microreactor

Modelling of the liquid chamber was established by connecting the gas phase reaction zone with the bulk liquid phase. The mass balance equation for the 4-propylguaiacol in the liquid phase is expressed as:

$$u_x \frac{\delta c_{4PG}}{\delta x} = D_i \left(\frac{\delta^2 c_{4PG}}{\delta x^2} + \frac{\delta^2 c_{4PG}}{\delta y^2} \right) \quad (3)$$

where c_{4PG} is the concentration of 4-propylguaiacol in the bulk liquid phase in mol/m^3, D_i is the molecular diffusion coefficient (m/s) in the bulk liquid, u_x is the liquid velocity in the axial direction.

The mass balance in the gas phase reaction zone is expressed as:

$$D_i \left(\frac{\delta^2 c_i}{\delta x^2} + \frac{\delta^2 c_i}{\delta y^2} \right) + u_x \frac{\delta c_i}{\delta x} = R \quad (4)$$

where *i* represents 4-propylguaiacol or H_2, and *R* incorporates the rate of reaction term. The molecular diffusion coefficient of 4-propylguaiacol (D_{4PG}) in the fluid was calculated using the Reddy-Doraiswamy correlation[18].

$$D_{4PG} = 1 \times 10^{-16} \left(\frac{T\sqrt{M_{4PG}}}{\mu V_{4PG}^{\frac{2}{3}}} \right) \quad (5)$$

where *T* is the temperature in K, M_{4PG} is the molecular mass of 4-propylguaiacol in g/mol, μ is the viscosity of 4-propylguaiacol in Pa·s and V_{4PG} is the molar volume of 4-propylguaiacol at normal boiling point in m^3/kmol[19]. The molecular diffusion coefficient of hydrogen (D_{H_2}) was obtained using the Wilke-Chang correlation[20].

$$D_{H_2} = 1.1728 \times 10^{-16} \frac{T\sqrt{\chi M_{4PG}}}{\mu V_{H_2}^{0.6}} \quad (6)$$

where χ is the association factor of 4-propylguaiacol, 1 for non-associated solvents, V_{H_2} is the molar volume of hydrogen at normal boiling point in m^3/kmol[21]. The boundary conditions

utilised for the pseudo-homogeneous model were as per the following:

at x = 0; $c_{H2} = c_{H_2,in}$, $c_{4PG} = 0$ (7)

at y = l_1; $c_{4PG,b} = H^* c_{4PG}$, $\frac{\delta c_{H_2}}{\delta y} = 0$ (8)

at x = 180, $\frac{\delta c_i}{\delta x} = 0$ (9)

at y = 0; $c_{4PG} = c_{4PG,in}$, $c_{H_2} = 0$ (10)

The mass balance equations coupled with the appropriate boundary conditions were solved using COMSOL Multiphysics® software version 5.3. The finalized geometry comprised of a mesh consisting of 4400 domain elements and 400 boundary elements, and 9,090 degrees of freedom was used, and the results were found to be mesh independent with a computational time of 5 seconds.

2.4 Detailed multiphase model

The previous pseudo-homogeneous model shown in section 2.2 was further enhanced to incorporate the catalyst particles on which the gas phase reaction occurs. The assumptions for the pseudo-homogeneous model are applicable to this detailed model, with the exception that the reaction zone in figure 1 is packed with solid spherical catalyst particles of the same size and shape. The mass balance equation for the species in the catalyst bed is expressed as:

$$u_x \frac{\delta c_i}{\delta x} = D_{i,A} \frac{\delta^2 c_i}{\delta x^2} + D_{i,T} \frac{\delta^2 c_i}{\delta y^2} - J_i S_b \quad (11)$$

where, $D_{i,A}$ and $D_{i,T}$ are the axial and transverse dispersion coefficients respectively, J_i is the molar flux of *i* into the catalyst particles, S_b is the specific surface area of the particles exposed to the reacting fluids in the packed bed (assuming randomly packed spherical particles) and is given by[22]:

$$S_b = S(1 - \varepsilon) \quad (12)$$

where, ε is the fractional voidage of the packed bed and *S* is the specific surface area, in m, of the particles. For spherical particles this is given by:

$$S = \frac{3}{r_p} \quad (13)$$

where, r_p is the catalyst particle radius.

An assumption of the film condition is realised at the pellet-fluid interface. The mass flux across this pellet-fluid interface into the pellet is potentially rate determined by the resistance to mass transfer on the bulk fluid side. This resistance can be expressed in terms of the external mass transfer coefficient:

$$J_i = h_i(c_i - c_{i,ps}) \quad (14)$$

$$h_i = \frac{Sh \cdot D_i}{2r_p} \quad (15)$$

$$Sc = \frac{\mu}{\rho \cdot D_i} \quad (16)$$

$$Re = \frac{2r_p \cdot \rho \cdot u_x}{\mu} \quad (17)$$

$$Sh = 2 + 0.552 Re^{1/2} Sc^{1/3} \quad (18)$$

where, $c_{i,ps}$ is the concentration of *i* at the catalyst particle surface and h_i is the external mass transfer coefficient. *Sc* is the Schmidt number, μ is viscosity of 4-propylguaiacol and ρ is the density of 4-propylguaiacol. *Re* is the particle Reynolds number[23]. *Sh* is the Sherwood number, which is based upon the Frössling correlation[24].

The chemical reaction which occurs inside (within) the pellets is incorporated into the mass balances with the Reactive Pellet Bed feature in COMSOL®. This feature has a predefined 1-D extra dimension on the normalised radius of the catalyst pellet particle ($r = r_{dim}/r_{pe}$). The mass balance inside the catalyst pellet is obtained by performing a shell balance across a spherical shell:

$$\frac{\delta}{\delta r}\left(r^2 D_{i,eff} \frac{\delta c_{i,p}}{\delta r}\right) = r^2 r_p R_{i,p} \quad (19)$$

where *r* is the catalyst particle radius (dimensionless), $D_{i,eff}$ is the effective diffusion coefficient of chemical species *i* in the catalyst pores, $c_{i,p}$ is the concentration of chemical species *i* in the catalyst particle in mol/m³. $R_{i,p}$ is the reaction source term (rate of reaction per unit volume of catalyst particle). The effective diffusivities of 4-propylguaiacol and hydrogen into the pores of the catalyst pellet are calculated by relating the diffusion coefficient to either the bulk or Knudsen diffusivity.

$$D_{i,eff} = \frac{D_{i,AB} \Phi_p \sigma_c}{\tau} \quad (20)$$

where, $D_{i,AB}$ is the bulk diffusivity of chemical species i, Φ_p is the pellet porosity, σ_c is the constriction factor and τ is the tortuosity. Typical values of the constriction factor, the tortuosity, and the pellet porosity are, respectively, σ_c = 0.8, τ = 3.0 and Φ_p = 0.4[25]. Boundary conditions used were as per the following:

at x = 0; $c_{H_2} = c_{H_2,in}$, $c_{4PG} = 0$ (21)

at y = l_1; $c_{4PG,b} = H^* c_{4PG}$, $\frac{\delta c_{H_2}}{\delta y} = 0$ (22)

at x = 180, $\frac{\delta c_i}{\delta x} = 0$ (23)

at y = 0; $c_{4PG} = c_{4PG,in}$, $c_{H_2} = 0$ (24)

at r = 1; $c_{i,p} = c_{i,ps}$ (25)

at r = 0; $\frac{\delta c_{i,p}}{\delta r} = 0$ (26)

Table 3: The list of parameters used for the CFD models

Symbol	Value	Units	Description
$c_{4PG,in}$	1.1	mol m^{-3}	4-propylguaiacol inlet concentration
$c_{H2,g}$	$\frac{P_{H2}}{RT}$	mol m^{-3}	Hydrogen concentration in the gas phase
υ	0.03-0.18	mL min^{-1}	4-propylguaiacol inlet flow rate
$F_{H2,in}$	30-120	cm^3 min^{-1}	Hydrogen inlet flow rate
H	l_1+l_2	mm	Reactor height
W	180	mm	Reactor width
l_2	0.762	mm	Reaction zone height
l_1	0.762×10^{-3}	mm	Liquid chamber height
D_{4PG}	9.995×10^{-8}	m^2 s^{-1}	Diffusion coefficient of 4-propylguaiacol in the bulk fluid[18, 19]
D_{H2}	1.23×10^{-8}	m^2 s^{-1}	Diffusion coefficient of hydrogen in the bulk fluid [15, 16]
$D_{4PG,eff}$	1.312×10^{-9}	m^2 s^{-1}	Effective diffusion coefficient of 4-propylguaiacol in the catalyst particle[25]
$D_{H2,eff}$	1.066×10^{-9}	m^2 s^{-1}	Effective diffusion coefficient of hydrogen in the catalyst particle[25]
ρ_b	580	kg m^{-3}	Density of catalyst bed
ρ_{pe}	750	kg m^{-3}	Density of catalyst pellet
ε_{pe}	0.4	-	Porosity of pellet
ε_b	$1 - \rho_b/\rho_{pe}$	-	Void fraction of catalyst bed
r_{pe}	1.1×10^{-4}	m	Radius of catalyst pellet
R	8.314×10^{-9}	m^3.bar ($K^{-1}mol^{-1}$)	Ideal gas constant
M_{4PG}	166.22	g mol^{-1}	Molecular weight of 4-propylguaiacol

The mass balance equations coupled with the appropriate boundary conditions were solved using COMSOL Multiphysics® software version 5.3. The finalized geometry comprised of a mesh consisting of 440,000 domain elements and 30,088 boundary elements, and 106,858 degrees of freedom was used, and the results were found to be mesh independent with a computational time of 12 seconds. The variables, which were used to solve the models, are shown in table 3.

3. Results and Discussion

3.1 Model validation

3.1.1. Effects of temperature

The results obtained from the CFD pseudo homogeneous and detailed models were compared to the experimental data. Both models were compared to experimental results for a microreactor operating at a pressure of 300 psig, and temperatures of 250-450 °C. The comparison between the simulated results and the experimental results give an indication towards the validity and robustness of the model. Figure 2 shows the comparison between the modelling and experimental results. The graph depicts the conversion of 4-propylguaiacol obtained for a temperature range of 250-450 °C with a good agreement between the experimental and obtained CFD (i.e. pseudo-homogeneous and detailed model) results.

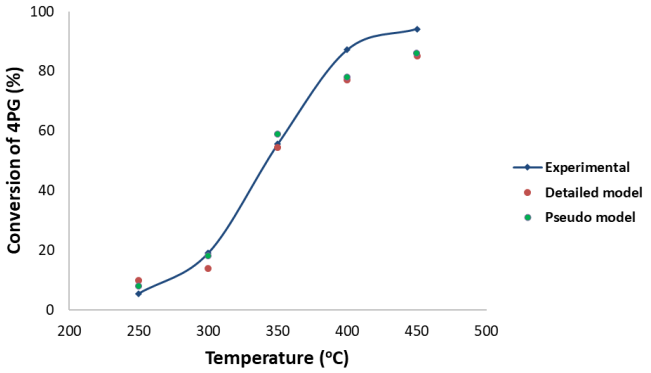

Figure 2: Comparison between model predicted results and experimental results: Pressure, 300 psig; gas phase, hydrogen; liquid phase, 4-propylguaiacol.

The results show that as the temperature increases, the conversion of 4-propylguaiacol also increases. For temperatures below 400 °C, there is a very good validation between the results; however, there is a slight deviation in the results at temperatures, which exceed 400 °C. This could be due to the fact that secondary side reactions are occurring within the microreactor[26], these reactions are not considered within the CFD modelling due to the lack of reaction kinetic data available. The predominant products from the HDO of 4-propylgauaicol using the presulfided-NiMo/Al_2O_3 catalyst are 4-propylphenol, 4-ethylphenol, 4-propylbenzene, phenols and cresols with insignificant quantities of benzene and toluene. The compound 4-propylphenol is solely brought to attention in this study because it has the highest selectivity.

3.1.2. Effects of hydrogen partial pressure

The effect of hydrogen partial pressure on the conversion of 4-propylguaiacol was investigated using the models developed in this work and were compared with the results from literature. The range of pressures used for the study varied from 240-480 psig at a constant reactor temperature of 400 °C with a constant residence time. The results in Figure 3 show that as the hydrogen partial pressure increases, the conversion of 4-propylguaiacol also increases. However, at pressures of approximately 400 psig, the conversion remains relatively constant. This is because at higher temperatures there is a maximum adsorption of hydrogen on the surface of the catalyst resulting in a stable conversion. The comparison in results between the CFD modelling and experimental show a very good agreement.

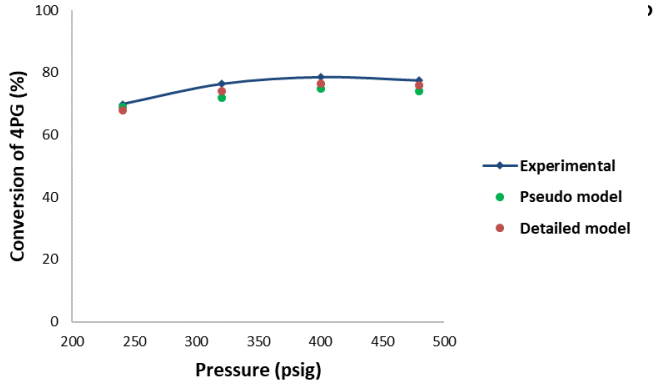

Figure 3: Effect of hydrogen inlet pressure on the conversion of 4-Propylguaiacol: Temperature, 400 °C; gas phase, hydrogen; liquid phase 4-propylguaiacol; gas phase, hydrogen.

3.1.3. Effects of liquid flow rate of 4-propylguaiacol

The effect of liquid flow rate on the conversion of 4-propylguaiacol was also studied using the proposed models. The liquid flow rate of 4-propylguaiacol varied between 0.03-0.15 mL min-1, and the remaining operating parameters were kept constant. The studies were performed at a temperature and pressure of 400 °C and 300 psig respectively. Figure 4 shows that as the liquid flow rate increases, the conversion of 4-propylguaiacol decreases. The reacting fluids spend a shorter time within the microreactor as the liquid flow rate decreases, hence the conversion declines. Both models predict a decreasing conversion profile with the liquid flow rate which is consistent with the dependence of conversion of a reactant upon space velocity. 4-propylguaiacol is only a reactant in the reaction network presented by the experimentalists[3], which cannot justify the existence of a maximum in the profile. This is also consistent with the findings and conclusions of the experimentalists[3], who also describe their experimental conversion profile as decreasing. We believe that the maximum in the experimental profile is an artefactual one and caused by small experimental errors. The deviation of the experimental conversion values is within in the experimental error range.

As the results obtained from the models are in agreement with the experimental findings[3], they demonstrate a good validation of our models.

Figure 5 shows the concentration profiles of 4-propylguaiacol in the bulk fluid phase across the transverse direction at different axial positions. It can be observed that the concentration of 4-propylguaiacol is highest at the initial axial positions of the microreactor, this is where the 4-propylguaiacol first encounters the hydrogen at the interface (at x=0; y=0). As the axial position of the microreactor progresses, the concentration decreases until eventually becoming stable. This is because, as the concentration of hydrogen increases along the axial direction of the microreactor, it will encounter greater concentrations of the 4-propylguaiacol, which results in a stable reactant conversion.

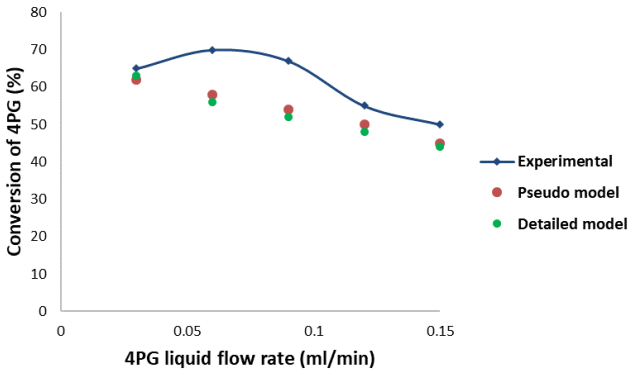

Figure 4: Effect of 4-propylguaiacol liquid flow rate on the conversion of 4-Propylguaiacol: Temperature, 400 °C; pressure, 300 psig; gas phase, hydrogen; liquid phase 4-propylguaiacol.

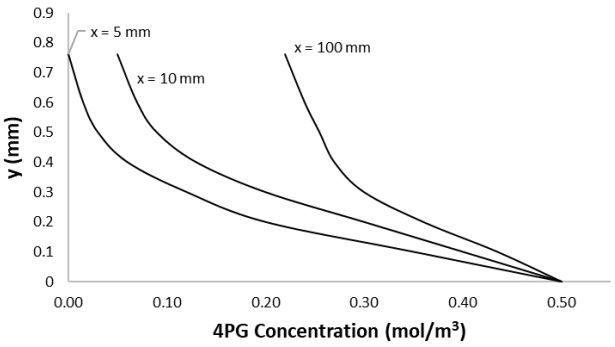

Figure 5: Concentration profiles of 4-propylguaiacol in the bulk fluid phase at a constant transverse direction and varying axial positions: Temperature, 400 °C; pressure, 300 psig; gas phase, hydrogen; liquid phase 4-propylguaiacol.

3.2. Kinetic studies

3.2.1 Rate analysis

The effect of hydrogen concentration on the rate of disappearance of 4PG was investigated using the detailed model. The hydrogen concentration varied between 0-0.15 mol/L, and the concentration of 4-propylguaiacol remained

constant at 1.1 mol/L. Three different temperatures of 350 °C, 300 °C and 250 °C were investigated to obtain the CFD modelling results. All other parameters were kept constant, and the conversion of the reactants was limited to a maximum of 10% in order to solely determine the reaction rates founded on the initial concentrations of the reacting fluids. Figure 6 shows the results obtained from the study. It can be observed that as the concentration of hydrogen increases, the rate of propylguaiacol also increases.

The effect of 4-propylguaiacol concentration on the rate of disappearance of 4-propylguaiacol was then investigated. The 4-propylguaiacol concentration varied from 0.1-2.1 mol/L, at constant hydrogen pressure of 208 psig. The three temperatures used for the study were 350 °C, 300 °C and 250 °C. Figure 7 shows the results obtained. It can be observed that at lower concentrations of 4-propylguaiacol the rate of propylguaiacol appears to increase. However, at higher concentrations, the rate remains relatively constant.

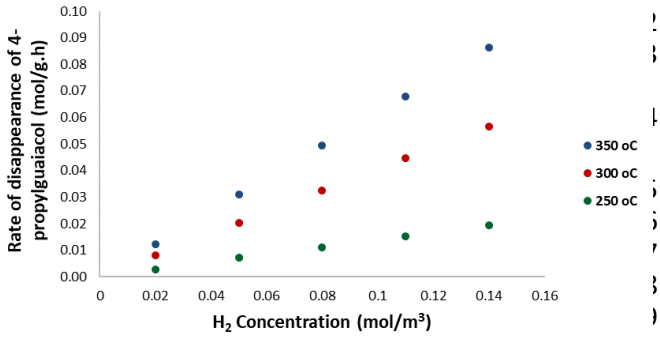

Figure 6: Effect of hydrogen concentration on the rate of 4-Propylguaiacol: Gas phase, hydrogen; liquid phase 4-propylguaiacol.

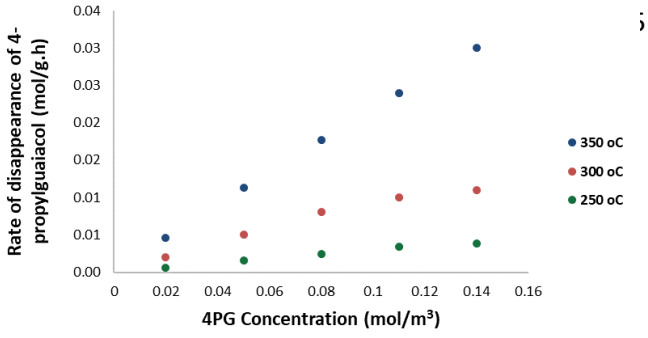

Figure 7: Effect of hydrogen concentration on the rate of 4-Propylguaiacol: Gas phase, hydrogen; liquid phase 4-propylguaiacol.

3.3 Internal and External mass transfer limitations

The heterogeneous detailed model incorporates the solid catalyst, and so it can ascertain the internal and external mass transfer resistances within the microreactor. The model will demonstrate which parameters lead to the reaction being diffusion limited or surface-reaction-limited. Using the CFD models to study the internal mass transfer limitations can also aid the determination of which factors enhance or diminish the mass transfer rates (affecting the apparent rate of reaction); therefore, an understanding of the optimisation of the HDO reaction can be achieved.

3.3.1 Internal mass transfer limitations

The concentration profiles of 4-propylguaiacol are presented in figure 8. The profiles were obtained at x = 90 mm, and varying reactor heights of y = 0.7; 0.5 and 0.2 mm, for a catalyst particle size of 75-150 µm. The internal mass transfer resistance is responsible for the concentration gradient within the catalyst particle. It can be deduced that the difference in concentration from the surface of the particle, to within the particle, is less than 5%. In addition, the model was simulated with constant reactor properties, and catalyst particle sizes which were halved and quartered. It was observed that there was no significant difference in the conversion of 4-propylguaiacol (less than 2%). The internal mass transfer limitation was further validated by calculating the Thiele modulus (Φ) for a particle size ranging from 70-160 µm by assuming the reaction to be pseudo-first-order with respect to 4-propylguaiacol and hydrogen[25].

$$\Phi = \frac{r_p}{3}\left(\frac{\rho_p \cdot (-r'_{4PG})}{D_e \cdot C_{H2}}\right)^{\frac{1}{2}} \qquad (27)$$

where ρ_p is the density of the catalyst pellet. The Thiele modulus was found to be approximately 0.5. For this value of the Thiele modulus, the effectiveness factor is found to be 1; which suggests that the reaction is surface-reaction-limited (overall rate of reaction is equal to the rate of reaction obtained from within the catalyst particle maintaining the same conditions as the particle surface). Therefore, from this study, it can be concluded that there is negligible internal mass transfer resistance. This conclusion coincides with that obtained from the experimental results.

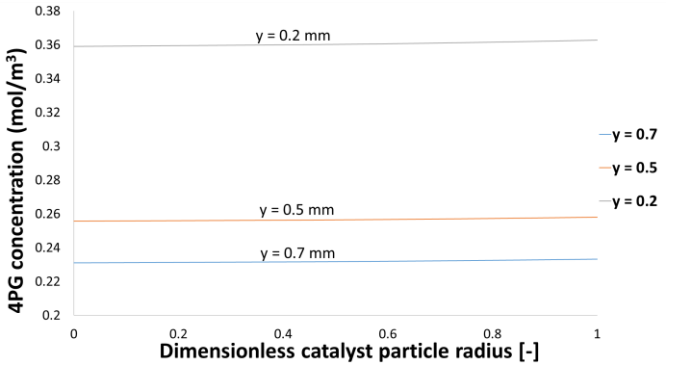

Figure 8: Concentration of 4-Propylguaiacol within the catalyst particles at x = 90 mm, generated from modelling: Gas phase, hydrogen; liquid phase 4-propylguaiacol; reaction temperature 400 °C.

The size of the catalyst particle was doubled and quadrupled to introduce pore diffusion limitations. Figure 9 shows the concentration profiles obtained at x = 90 mm, and varying reactor heights of y = 0.7; 0.5 and 0.2 mm. The introduction of the intraparticle transport resistances is responsible for the

steeper concentration profile. This makes microreactors desirable due to their shorter lengths, which allows the use of smaller catalyst particles, which may not usually be feasible in conventional macroscopic reactors.

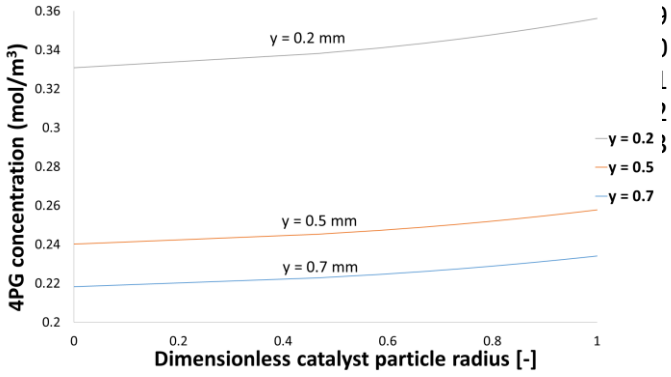

Figure 9: Concentration of 4-Propylguaiacol within the catalyst particles at x = 90 mm, generated from modelling: Gas phase, hydrogen; liquid phase 4-propylguaiacol; reaction temperature 400 °C.

The comprehensive heterogeneous model was used to obtain the internal effectiveness factor. This provides an indication of the relative importance of diffusion and reaction limitations. The effectiveness factor is regarded as the ratio between the actual overall rate of reaction, and the rate of reaction that would occur if the interior surface of the pellet were exposed to the external surface conditions[25]. The effectiveness factor for a spherical catalyst particle following a first-order reaction can be obtained as:

$$\eta = \frac{3}{\Phi^2}(\Phi \coth \Phi - 1) \qquad (28)$$

Figure 10 shows a plot of the effectiveness factor against the Thiele Modulus using the detailed model. For the catalyst pellet sizes between 75-150 µm, the Thiele Modulus is approximately less than 1, this corresponds to an effectiveness factor of unity which suggests negligible internal mass transfer resistances. However, increasing the particle sizes results in a decrease in the effectiveness factor, suggesting that the reaction is becoming diffusion-limited within the pellet.

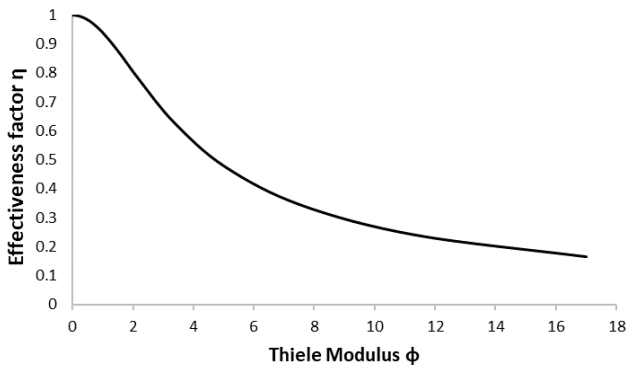

Figure 10: A plot of the effectiveness factor as a function of the Thiele modulus.

Figure 11 shows a plot of the conversion of 4-propylguaiacol and the liquid flow rate for the pseudo-homogeneous model, detailed model and the detailed model with a catalyst size of 220 µm. It can be observed that the reactant conversion decreases with the larger catalyst sizes. From the modelling results, the overall rate of reaction could be enhanced by decreasing the catalyst particle size; increasing the internal surface area; increasing the temperature; and increasing the concentration.

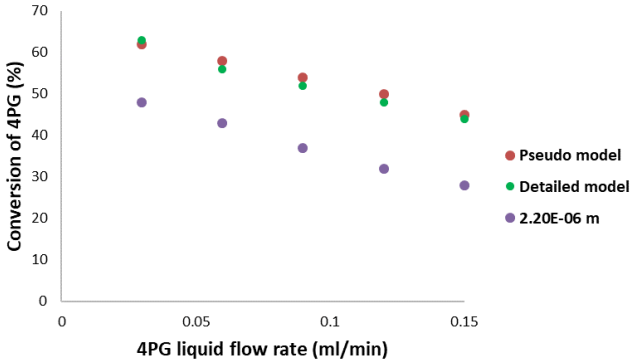

Figure 11: Effect of 4-propylguaiacol liquid flow rate on the conversion of 4-propylguaiacol for different model configurations: Temperature, 400 °C; pressure, 300 psig; gas phase, hydrogen; liquid phase 4-propylguaiacol.

A study of comparison between the pseudo-homogeneous and detailed model was conducted. Figure 12 shows the conversion of 4-propylguaiacol against the liquid flow rate for the detailed model, comprising of catalyst particle sizes ranging between 220-500 µm, and the pseudo-homogeneous model. The results show that as the pellet sizes increase, the reactant conversion decreases because of the diffusion limitations within the particle. The reaction rates obtained from the pseudo-homogeneous model were multiplied with the effectiveness factor to obtain the results shown in figure 12. There is a good agreement between the results which demonstrates the validity and robustness between the two models. As a result, either model can be utilised to demonstrate the catalytic hydrodeoxygenation of bio-oil to produce desirable results.

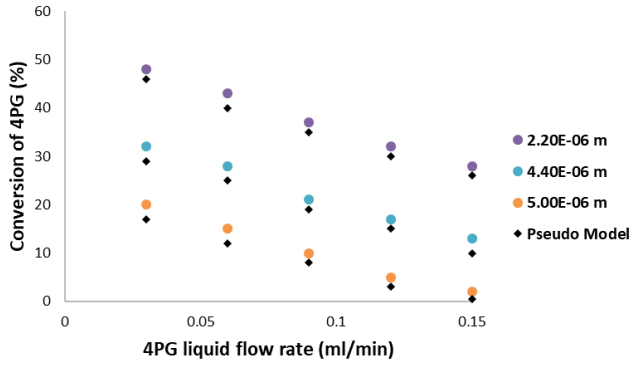

Figure 12: Effect of 4-propylguaiacol liquid flow rate on the conversion of 4-propylguaiacol for different catalyst pellet sizes: Temperature, 400 °C; pressure, 300 psig; gas phase, hydrogen; liquid phase 4-propylguaiacol.

3.3.2 External mass transfer limitations

The external mass transfer resistance was then investigated. The hydrodeoxygenation reaction involves the diffusion and mass transfer of hydrogen gas into the 4-propylguaiacol liquid phase, and subsequently diffusion through the liquid phase to the proximate area of the catalyst particle. In order to investigate the resistance to the diffusion across the boundary layer, the concentration surrounding the catalyst particle should be compared to the concentration on the surface of the particle. Figure 13 shows the bulk concentrations of 4-propylguaiacol compared to the concentrations obtained from the surface of the catalyst particle. The concentrations of 4-propylguaiacol in the bulk are found to be less than 2% when compared to the concentrations on the surface of the catalyst particle. It can be deduced that there is a negligible resistance to mass transfer, and this agrees with the experimental results obtained from Joshi and Lawal (2013).

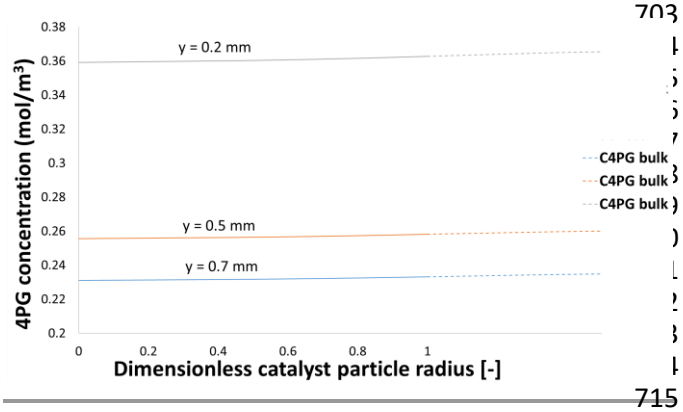

Figure 13: Comparison between concentration of 4-Propylguaiacol within the catalyst particles and in the bulk at x = 90 mm, generated from modelling: Gas phase, hydrogen; liquid phase 4-propylguaiacol; reaction temperature 400 °C.

4. Conclusions

The modelling results obtained from the CFD study for the catalytic HDO of 4-propylguaiacol to 4-propylphenol have demonstrated a sound validation with the experimental data obtained from literature [3]. The slight deviations in results at temperatures greater than 350 °C could owe to the fact that the results closely follow the % yield of other major reaction products. The secondary side reactions are not considered in this work (due to the lack of kinetic data available). Therefore, the models developed could have slight limitations at higher temperatures because of the previously mentioned reasons; however, this would be overcome by the development of more complex kinetic models which account for the side reactions interacting with the HDO of 4-propylguaiacol to 4-propylphenol. Further model validations were demonstrated by the effects of pressure and liquid flow rate illustrate a good validation with the experimental data. It can be observed that for this specific reaction, the conversion of 4-propylguaiacol increased with increasing temperature and pressure; however, increasing the liquid flow rate appears to decrease the reactant conversion.

The detailed model further allowed the investigation of the concentrations of hydrogen and 4-propylguaiacol on the rate of 4-propylguaiacol. The model results demonstrated that as the concentration of these reactants increased, the rate of disappearance of 4-propylguaiacol also increased. In addition, the detailed model gave rise to the characterisation and evaluation of the reaction-coupled transport phenomena taking place within the catalyst bed in the microreactor. The internal and external mass transfer limitations were investigated by obtaining concentration profiles within the individual catalyst particle. It was concluded that there were negligible internal and external mass transfer resistances, which agreed with the experimental results. In addition, the study of pore diffusion limitations suggested a good agreement between the pseudo-homogeneous and detailed heterogeneous models. It can be observed that both models performed similarly when being compared to the experimental data. This indicates the validity and robustness between the models; hence, either model has the ability to predict the catalytic HDO of bio-oil in microreactors. The heterogeneous model has allowed the investigation of pore diffusion limitations by predicting a range of values of the Thiele Modulus at which this occurs. It has shown how this affects the reaction; and gives rise to the study of particle fluid transport phenomena, which aids the understanding of internal and external mass transfer resistances. Performing numerical simulation studies is valuable as it provides an understanding of parameter optimisation and predicting the HDO of other various compounds present in bio-oil, which would be time consuming and costly to do on an experimental basis.

As the HDO reaction of lignin-derived compounds has not been studied extensively, this model provides a basis to predict and enhance the comprehensive understanding of the HDO reaction in various other lignin-derived compounds in bio-oil. Furthermore, microreactors have demonstrated various benefits[11, 27, 28] compared to conventional reactors, and so future research should be directed towards investigating the scalability of microreactors to be used on an industrial scale.

Conflicts of interest

There are no conflicts to declare.

Acknowledgements

The authors would like to thank London South Bank University, School of Engineering, for the PhD funding support.

References

1. G. Özsin and A. E. Pütün, *Energy Conversion and Management*, 2017, **149**, 675-685.
2. B. Biswas, N. Pandey, Y. Bisht, R. Singh, J. Kumar and T. Bhaskar, *Bioresource technology*, 2017, **237**, 57-63.
3. N. Joshi and A. Lawal, *Industrial & Engineering Chemistry Research*, 2013, **52**, 4049-4058.

4. S. Hawash, J. Y. Farah and G. El-Diwani, *Journal of Analytical and Applied Pyrolysis*, 2017, **124**, 369-372.
5. L.-j. LIU, Y.-g. LIU, G. Xiang, R.-q. ZHANG and Y.-p. ZHAI, *Journal of Fuel Chemistry and Technology*, 2017, **45**, 932-938.
6. H. Lee, Y.-M. Kim, I.-G. Lee, J.-K. Jeon, S.-C. Jung, J. Do Chung, W. G. Choi and Y.-K. Park, *Korean Journal of Chemical Engineering*, 2016, **33**, 3299-3315.
7. M. Saidi, F. Samimi, D. Karimipourfard, T. Nimmanwudipong, B. C. Gates and M. R. Rahimpour, *Energy & Environmental Science*, 2014, **7**, 103-129.
8. H. Lee, H. Kim, M. J. Yu, C. H. Ko, J.-K. Jeon, J. Jae, S. H. Park, S.-C. Jung and Y.-K. Park, *Scientific reports*, 2016, **6**, 1-8.
9. M. L. Patil, A. M. Lali and A. K. Dalai, *Asia-Pacific Journal of Chemical Engineering*, 2019, **14**, e2317.
10. H. Taghvaei and M. R. Rahimpour, *Process Safety and Environmental Protection*, 2019, **121**, 221-228.
11. S. Hafeez, G. Manos, S. Al-Salem, E. Aristodemou and A. Constantinou, *Reaction Chemistry & Engineering*, 2018, **3**, 414-432.
12. S. G. Newman and K. F. Jensen, *Green Chemistry*, 2013, **15**, 1456-1472.
13. M. D. Subramanyam, A. R. Gollakota and N. Kishore, *RSC Advances*, 2015, **5**, 90354-90366.
14. A. R. Gollakota, M. D. Subramanyam, N. Kishore and S. Gu, *RSC Advances*, 2015, **5**, 41855-41866.
15. Q. Xiong, Y. Yang, F. Xu, Y. Pan, J. Zhang, K. Hong, G. Lorenzini and S. Wang, *ACS Sustainable Chemistry & Engineering*, 2017, **5**, 2783-2798.
16. Q. Xiong, F. Xu, E. Ramirez, S. Pannala and C. S. Daw, *Fuel*, 2016, **164**, 11-17.
17. G. W. Huber, S. Iborra and A. Corma, *Chemical reviews*, 2006, **106**, 4044-4098.
18. K. Reddy and L. Doraiswamy, *Industrial & Engineering Chemistry Fundamentals*, 1967, **6**, 77-79.
19. C. L. Yaws, *Journal*, 2010.
20. C. Wilke and P. Chang, *AIChE Journal*, 1955, **1**, 264-270.
21. C. L. Yaws, *Yaws' critical property data for chemical engineers and chemists*, Knovel, 2012.
22. J. Richardson, J. Harker and J. Backhurst, *Chemical engineering*, 2002, **2**, 191-236.
23. S. Fogler, *Inc., NJ*, 1999.
24. N. Frössling, *Gerlands Beiträge zur Geophysik*, 1938, **52**, 170-216.
25. H. Fogler, *Journal*, 2006.
26. M. Nowakowska, O. Herbinet, A. Dufour and P.-A. Glaude, *The Journal of Physical Chemistry A*, 2018, **122**, 7894-7909.
27. A. Constantinou, F. Ghiotto, K. F. Lam and A. Gavriilidis, *Analyst*, 2014, **139**, 266-272.
28. X. Sun, A. Constantinou and A. Gavriilidis, *Chemical Engineering and Processing: Process Intensification*, 2011, **50**, 991-997.

